ChemPubSoc Europe

DOI: 10.1002/ejic.201501376

EurJIC European Journal of Inorganic Chemistry

Communication

Supported Nanoparticles

Gold Nanoparticle@Polyhedral Oligomeric Silsesquioxane Hybrid Scaffolds in Microfluidic Format – Highly Efficient and Green Catalytic Platforms

Pascal Scholder,[a] Martina Hafner,[b] Achim W. Hassel,[b] and Ivo Nischang*[c,d]

Abstract: We report on the preparation of new hybrid organic–inorganic multiporous monolithic capillary columns carrying gold nanoparticles of 5, 10, 50, and 100 nm size and their use as flow-through catalytic platforms for aqueous liquid-phase reduction reactions. We found that the flow-through performance of the reactors depends not only on the size of the gold nanoparticles but also on the interplay of the pore size of the scaffolds and the catalytically available gold surface within the system, that is, loading an increased number of gold nanoparticles of smaller size does not necessarily result in strictly improved performance. This indicates the importance of the interplay between the nanopore size of the scaffolds and the catalytically active gold surface existing within the system. Demonstration of the highly efficient catalytic flow-through operation within seconds and the repeated use of the reactors without loss of performance indicates their excellent suitability as microfluidic device elements.

Introduction

The area of nanoparticulate colloidal matter prepared from noble metals has diversified rapidly with the recognition of these materials as useful tools for optics, sensing, catalysis, release agents, and so on.[1] This diversity is associated to their favorable surface-to-volume ratio as well as their related and interesting physicochemical properties.[2] Use of colloidal matter, providing large surface-to-volume ratios, exploits specific and desirable assets of the materials. These assets emerge from associated surface energies that vary with surface crystal orientation and facets, curvature, and topology. With the availability of colloidal gold, whose preparation was pioneered as early as the 1950s,[3] its catalytic properties were soon recognized and used in technological applications. In the meanwhile, such colloidal gold nanoparticles are commercially available in a variety of shapes and sizes, as well as with associated surface topographies, for a range of applications from biomedical studies to analytical engineering implementations.[1,4]

The catalytic activity of colloidal gold has mainly been explored for electron-transfer-associated reactions,[5] among other catalytic uses.[6] A desirable asset of colloidal nanoparticles is their good dispersibility in solution, if appropriately stabilized. In fact, immobilizing such particles on suitable supports provides an additional diversity in their microengineering applicability.[7] Benefits are easy removal from reaction solutions or flow-through operations, re-use for catalytic implementations, and prevention from agglomeration of individual nanoparticle entities. We herein report the first preparation of suitable, robust, highly porous, and easy-to-handle monolithic hybrid supports,[8] carrying a well-explored gold nanoparticle load and catalytically active surface. These highly porous scaffolds enable liquid flow at low back pressure[8c] and demonstrate facile and robust re-usability without any sign of clogging, together with excellent operational stability.

Results and Discussion

We describe the preparation of hybrid organic–inorganic monolithic materials[8b] in situ in the confines of 100 μm I.D. fused silica capillaries (Figure 1). The pendant vinyl groups inherently existing in these multiporous scaffolds[8] are then functionalized in situ with 1,3-propanedithiol by means of thiol–ene addition followed by reduction of the disulfides by a dithiothreitol solution. The pendant thiol groups allow the establishment of strong thiol–gold interactions to anchor gold nanoparticles of various sizes. This was achieved by simply flushing colloidal solutions of spherical gold nanoparticles through the hybrid monoliths until the effluent appeared to have the same color as that of the solution pumped into the capillaries (Figure 1).

[a] *Institute of Polymer Science, Johannes Kepler University Linz, Altenberger Str. 69, 4040 Linz, Austria*
[b] *Christian Doppler Laboratory for Combinatorial Oxide Chemistry, Institute for Chemical Technology of Inorganic Materials, Altenberger Straße 69, 4040 Linz, Austria*
[c] *Jena Center for Soft Matter (JCSM), Friedrich Schiller University Jena, Philosophenweg 7, 07743 Jena, Germany*
[d] *Laboratory of Organic and Macromolecular Chemistry (LOMC), Friedrich Schiller University Jena, Humboldtstr. 10, 07743 Jena, Germany*
E-mail: ivo.nischang@uni-jena.de

Supporting information for this article is available on the WWW under http://dx.doi.org/10.1002/ejic.201501376.

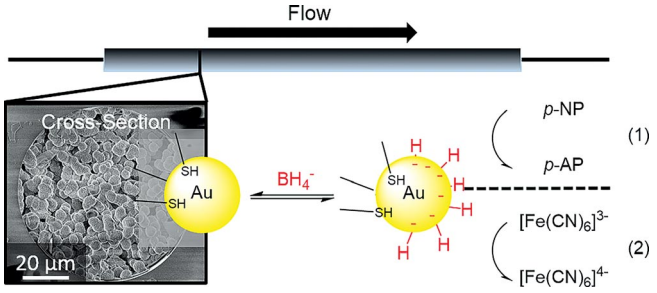

Figure 1. Flow set-up, SEM cross-section of hybrid monolithic flow-through structure in 100 µm I.D. fused silica capillaries carrying gold nanoparticles, as well as model catalytic reduction reactions (1) and (2) in an aqueous fluid phase containing sodium borohydride.

Table 1. Determined mass, number of particles, and surface of gold per 13 cm length of 100 µm I.D. capillary containing porous hybrid polymer.

Catalyst	Size (nm)[a]	m_{gold} (ng)[b]	Number[c]	Surface (µm²)[d]
1	5	19.3	15240.0×10^6	1196.9×10^3
2	10	8.3	824.0×10^6	258.9×10^3
3	50	6.9	5.5×10^6	42.9×10^3
4	100	15.5	1.5×10^6	48.3×10^3

[a] Size of immobilized gold nanoparticles as provided by the manufacturer. [b] Determined by ICP-MS. Samples were obtained by flushing the gold-containing monoliths with aqua regia as explained in detail in the Supporting Information. [c] Based on the assumption that the determined mass of gold consists of particles of a given size and spherical shape; calculated by using of 19.32 g cm^{-3} for the density of gold. [d] Calculated overall surface of the particles based on their number and size assuming spherical shape.

Figure 2 shows scanning electron microscopy (SEM) images of a single globular feature (example shown in Figure 1) of the as-prepared and washed pristine multiporous hybrid materials (Figure 2a) as well as those of variants carrying gold nanoparticles with sizes of 5 (catalyst **1**), 10 (catalyst **2**), 50 (catalyst **3**), and 100 nm (catalyst **4**). In images b, c, d, and e, the existence of colloidal gold is clearly indicated. In order to assess the amount of gold bound to the hybrid scaffold, we washed catalysts **1**–**4** with freshly prepared aqua regia and measured the gold content by inductively coupled plasma mass spectrometry (ICP-MS) (for details, see Supporting Information). The results of this analysis (Table 1) clearly suggest that a larger number of gold nanoparticles (recalculated from the mass of gold loaded on the scaffold) of smaller size can be loaded on identical pristine hybrid polymers. This increased particle load (over three orders of magnitude) is enabled by an increased available surface for the gold nanoparticles to associate to thiol groups. Smaller particles are likely to further ingress into the multiporous hybrid polymer structure with a significant population of mesopores that are smaller than 10–20 nm (Figure S2). This situation also explains why the number of loaded gold nanoparticles of 10, 50, and 100 nm size (catalysts **2**–**4**, Table 1) is significantly lower than that of nanoparticles of 5 nm size. Interestingly, however, the total gold surface area estimated per unit of capillary length is similar for the 50 (catalyst **3**) and 100 nm (catalyst **4**) nanoparticles (Table 1).

Nanoparticles of such size do not significantly ingress into the nanoporous hybrid polymer structure. This allows for a comparison of the performance of the prepared flow-through catalysts with various sizes of bound gold nanoparticles at a close-to-equivalent catalytically active surface area (vide infra).

It is well established in the literature that the catalytic activity of colloidal gold is dependent on the size of the gold nanoparticles.[7] Qualitatively, this was also observed in the present study with batch solution experiments of the studied reactions with diluted citrate-stabilized pristine gold nanoparticles of the same size as those immobilized on the solid monolithic hybrid supports. We performed experiments on identical gold surfaces with various gold nanoparticle concentrations, leaving other reaction conditions unchanged (Figure S4). The results reaffirm that the performance of smaller gold nanoparticles (5 and 10 nm) is clearly superior to that of larger gold nanoparticles (50 and 100 nm), while an overall trend of an improved apparent catalytic performance is found toward smaller particle sizes, a situation well in agreement with literature reports.[7] Estimated apparent rate constants from Figure S4b are in the same range as those typically found in the literature,[5b] which allows us to gauge the performance of the flow reactors.

When looking at the performance of our flow reactors (catalysts **1**–**4**) with a determined porosity of 82 % (see Supporting Information), we consistently found high conversions of *p*-nitrophenol and high yields of *p*-aminophenol at very low fluid contact times of a mere 1 min (Figure 3a). Catalyst **2** has the best performance (with near complete 100 % yield for *p*-nitrophenol within a timescale of 7–14 s), followed by catalyst **1**, and then by catalysts **3** and **4**. Importantly, the total amount of gold surface per unit volume of the capillary varies and spans more than one order of magnitude (Table 1). This situation can simply be explained by a significantly different ingression of gold nanoparticles into the multiporous hybrid support with gold-nanoparticle-size-dependent surface-to-capillary volume ratio.

In longer-timescale experiments (example of catalyst **2**), we observed a decrease in the yield during continuous operation (Figure 3b). In order to test whether this is associated to a loss in catalytic activity or structural changes in the reactor, we

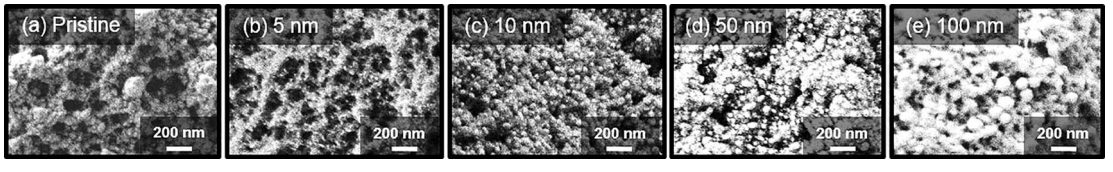

Figure 2. SEM images of the single globular features of the vinylPOSS hybrid polymers with an example capillary-scale cross-section shown in Figure 1 for (a) the pristine hybrid polymer indicating an appreciable amount of nanopores, and (b–e) for gold-nanoparticle-immobilized variants (catalysts **1**–**4**) clearly showing the internal structures with gold nanoparticles.

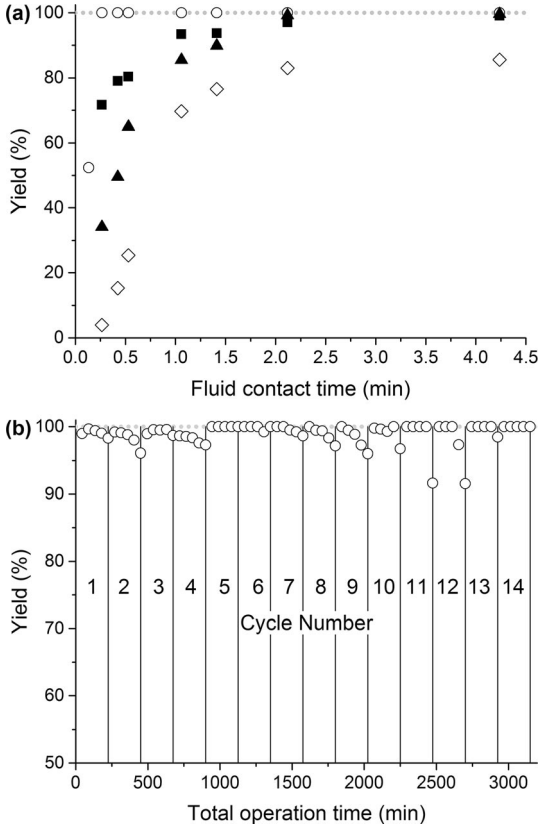

Figure 3. (a) Impact of fluid contact time in the reactors on the yield obtained for the catalytic reduction of *p*-nitrophenol with catalyst **1** (filled squares), catalyst **2** (empty circles), catalyst **3** (filled triangles), and catalyst **4** (empty diamonds). (b) Long-term stability of catalyst **2** in the steady state at a fluid contact time of 1 min and monitored over several reaction cycles with an overnight washing step and fresh reactant solutions provided after each cycle. Reactor length: 13 cm. Other conditions: 0.3×10^{-3} mol L^{-1} *p*-nitrophenol in water containing sodium borohydride (30×10^{-3} mol L^{-1}). The reactions were performed at a temperature of $T = 25$ °C.

flushed catalyst **2** after each cycle shown in Figure 3b overnight with deionized water. This was followed by operation with fresh reactant solutions, and this led to the re-establishment of catalytic performance, indicating that the structure of the catalytic material remains unaffected for at least 14 cycles, one cycle being performed each day. This refers to a total reactor volume of roughly 2500 under catalytic conditions. We believe that the yield decrease is associated to the instability of the sodium borohydride in the non-buffered reactant solution, which is continuously delivered by a loaded syringe over significant timescales.[9] This instability also raises the pH of the non-buffered solution over time.

Coming back to a discussion of catalytic performance and the size of the gold nanoparticles in solution and flow experiments, we find a similar relationship between gold nanoparticle size and catalytic performance (expressed in mol s^{-1} based on the same fluid contact time) for catalysts **1**–**4**, except that the best results were observed for a gold nanoparticle size of 10 nm, that is, catalyst **2** (Figure 4a). Repeatedly, catalyst **1** shows clearly decreased performance at the same fluid contact time. This may have a simple explanation because the larger content of gold nanoparticles emanates from their more pronounced ingression into the nanoporous structure of the hybrid polymer. Increasing confinement by the hybrid polymer then leads to a possibly reduced active gold nanoparticle surface that is accessible to the reactants to undergo electron-transfer reactions. Though the estimated surface area of colloidal gold is very similar for catalysts **3** and **4** (Table 1), catalyst **3** clearly performs better (Figure 4a), an aspect that can be attributed to a size effect of the particles.

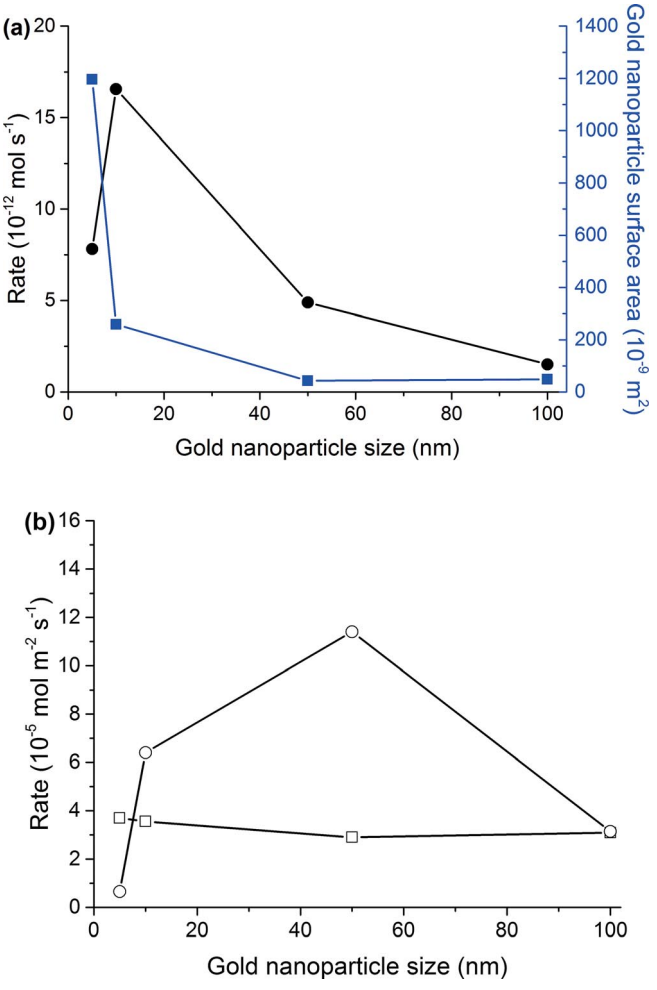

Figure 4. (a) Rate of reduction of *p*-nitrophenol by catalysts **1**–**4** calculated for a fluid contact time of 0.42 min (Figure 3a), except that for catalyst **2**, which was calculated for a fluid contact time of 0.13 min, together with the theoretical gold surface area for catalysts **1**–**4** (from Table 1) versus nanoparticle size. (b) Rate of reduction of *p*-nitrophenol with catalysts **1**–**4** in flow normalized by the estimated gold surface area (empty circles) together with that for the batch solution experiments (empty squares) at a reaction time of 5.3 min versus nanoparticle size. The reactions were performed at a constant temperature of $T = 25$ °C in both cases.

To deepen this insight, we had a look at the gold-surface-area-normalized rate of conversion (expressed in mol s^{-1} m^{-2}) per flow reactor, which is by far much worse than that in the solution experiment for catalyst **1** (Figure 4b), that is, roughly by an order of magnitude. Also this value indicates that a significant amount of the estimated colloidal gold surface (Table 1, Figure 4a) remains catalytically inactive for catalyst **1**, while catalyst **2** shows better performance than that in the solution experiment for this qualitative comparison. Interestingly, the use

of 50 and 100 nm gold nanoparticles leads to excellent performance again when the estimated surface area of gold is taken into account: the performance is at least comparable to that in the batch solution experiments (Figure 4b). Such nanoparticles are too small to significantly ingress into the hybrid polymer structure and are primarily located on the external surface of the structural features and close to the micrometer-sized flow-through pores (e.g. Figures 1, 2d, and 2e). Transport of reactants and products to and from the catalytically active gold surface is most efficient without the necessity to undergo hindered diffusion in pools of stagnant fluid.

The observation described above demonstrates for the very first time that a careful tailoring of the nanoporous structure of the scaffold very much impacts the gold load and the overall apparent catalytic performance, and yet it can be clearly enhanced with respect to that of batch solution experiments when performance is estimated per gold surface area, an aspect clearly attributable to the continuous operation of the catalytic reactions. This is because fresh reactant is continuously supplied to the reactor and the resultant product is removed. We find that catalyst **2** shows the best combination of gold nanoparticle load, nanoparticle size, and catalytically active surface (Figures 3a and 4b).

Having shown that the materials presented here possess excellent catalytic activity in the typical reduction reaction of *p*-nitrophenol, we also show their utility for the reduction of hexacyanoferrate(III). Since the reaction is rapid, we chose a pH value of 11.5 (adjusted with sodium hydroxide), which drastically increases the half-life of sodium borohydride.[9] Figure 5 shows results for the pristine polymer (used for thiol–ene addition and gold conjugation, Figure 2a). We consistently found no reduction reaction on the pristine material at increased sodium borohydride concentrations varying from 0.4 to 80×10^{-3} mol L^{-1}, the latter being more than twice the equimolar amount of that of hexacyanoferrate(III) (empty squares in Figure 5). On the gold-carrying scaffold catalyst **2** (Figure 2c), we found an increased conversion at increased sodium borohydride concentration under otherwise the same conditions as those for the pristine material (filled squares in Figure 5). The conversion asymptotically approaches values between 90 and 100 % at an excess amount of sodium borohydride. This situation is consistent with the typical assumption made in the literature that the reaction rate constant becomes independent of sodium borohydride concentration at concentrations much larger than those of hexacyanoferrate(III).[1a] Furthermore, it elegantly shows the catalytic activity of the immobilized gold nanoparticles.

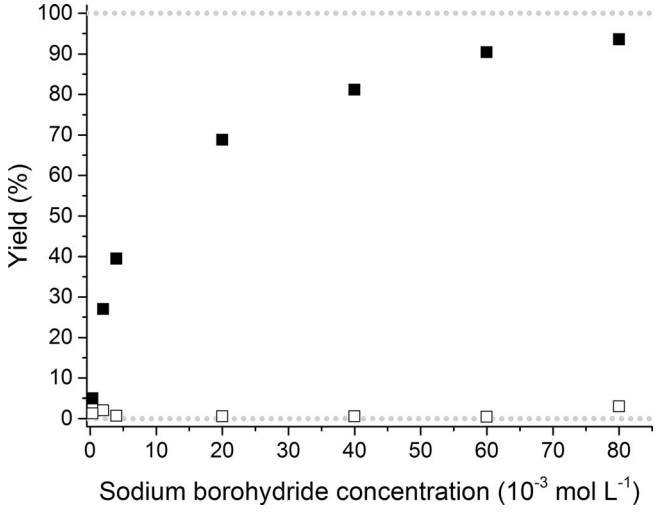

Figure 5. Impact of the sodium borohydride concentration on the yield obtained for the reduction of 40×10^{-3} mol L^{-1} hexacyanoferrate(III) at a pH = 11.5 (adjusted with NaOH) and a constant fluid contact time of 1 min by the pristine hybrid polymer (empty squares) and by catalyst **2** (filled squares). The reactions were performed at a constant reactor temperature of T = 25 °C.

Conclusion

In summary, we have demonstrated the preparation of gold nanoparticle@polyhedral oligomeric silsesquioxane hybrid scaffolds, with a set of gold nanoparticles ranging from 5 to 100 nm in size, and elucidated their use as efficient platforms for green synthetic applications in solely aqueous fluid phases. Our results show that these materials can be highly efficient catalytic platforms with robustness and re-usability over many catalytic cycles in continuous flow operation (Figure 3b). The overarching best performance is achieved with gold nanoparticles of size 10 nm (catalyst **2**). This is substantiated by the yield versus fluid contact time curves (Figure 3a) as well as the related performance characteristics (Figure 4). The results demonstrate that a careful combination of the porous structure of the scaffold and the chosen gold nanoparticle size drastically impacts the overall catalytic performance.

Our study further hints toward future endeavors for this type of reactors for catalytic screening applications involving colloidal matter as well as the integration of the prepared devices into more advanced microengineering platforms. In the present case, the scaffold shows significant hydrophobicity due to the alkyl linkages between the POSS cages. We currently explore the option to modify the pristine polymer with more hydrophilic dithiol linkers that will certainly lead to a better solvation of the material in an aqueous phase and, consequently, may lead to a potential impact on the catalytically active internal structure due to solvation and swelling effects. Such an approach should be accompanied by an advanced characterization of the porous structure in the solvated state.[10] Related effects may influence the ingression of gold nanoparticles into the hybrid polymer structure and also the overall catalytically active gold surface area provided by these microfluidic device elements that allow for operation timescales in the order of seconds.

Experimental Section

Porous hybrid monolithic scaffolds were prepared by a single-step molding process involving covalent anchorage to the confining capillary. Subsequently, the scaffolds were modified with pendant thiol groups, used as anchor for the gold nanoparticles, to prepare ready-to-use catalytic reactors operated in a continuous fashion for the two studied reactions. The performance of the reactors was monitored off-line with liquid chromatography. The analytical deter-

mination of the amount of gold within the reactors was performed by ICP-MS after dissolution with aqua regia. Further experimental details of scaffold preparation, modifications, and catalytic reactions as well as analytical studies on the materials and their results are provided in the Supporting Information.

Acknowledgments

This work was supported by the Austrian Science Fund (FWF) under project no. [P24557-N19]. The financial support by the Austrian Federal Ministry of Science, Research and Economy, and the National Foundation for Research, Technology and Development through the Christian Doppler Laboratory for Combinatorial Oxide Chemistry (COMBOX) is gratefully acknowledged.

Keywords: Continuous flow reactors · Supported catalysts · Nanoparticles · Gold · Organic–inorganic hybrid composites · Miniaturization

[1] a) P. Hervés, M. Pérez-Lorenzo, L. M. Liz-Marzán, J. Dzubiella, Y. Lu, M. Ballauff, *Chem. Soc. Rev.* **2012**, *41*, 5577–5587; b) Y. Mikami, A. Dhakshinamoorthy, M. Alvaro, H. García, *Catal. Sci. Technol.* **2013**, *3*, 58–69; c) J. Liu, S. Ma, Q. Wei, L. Jia, B. Yu, D. Wang, F. Zhou, *Nanoscale* **2013**, *5*, 11894–11901; d) S. Wang, J. Zhang, P. Yuan, Q. Sun, Y. Jia, W. Yan, Z. Chen, Q. Xu, *J. Mater. Sci.* **2015**, *50*, 1323–1332; e) I. Biondi, G. Laurenczy, P. J. Dyson, *Inorg. Chem.* **2011**, *50*, 8038–8045; f) Y. Du, H. Chen, R. Chen, N. Xu, *Appl. Catal. A* **2004**, *277*, 259–264; g) M. Al-Naji, A. M. Balu, A. Roibu, M. Goepel, W. Einicke, R. Luque, R. Gläser, *Catal. Sci. Technol.* **2015**, *5*, 2085–2091; h) Q. Xiao, S. Sarina, A. Bo, J. Jia, H. Liu, D. P. Arnold, Y. Huang, H. Wu, H. Zhu, *ACS Catal.* **2014**, *4*, 1725–1734; i) D. Quesada-Gonzalez, A. Merkoci, *Biosens. Bioelectron.* **2015**, *73*, 47–63; j) H. Liu, J. Liu, S. Li, L. Chen, H. Zhou, J. Zhu, Z. Zheng, *Opt. Commun.* **2015**, *352*, 148–154.

[2] a) Md. H. Rashid, T. K. Mandal, *Adv. Funct. Mater.* **2008**, *18*, 2261–2271; b) F. Lin, R. Doong, *Appl. Catal. A* **2014**, *486*, 32–41; c) T. Benkó, A. Beck, K. Frey, D. F. Srankó, O. Geszti, G. Sáfrán, B. Maróti, Z. Schay, *Appl. Catal. A* **2014**, *479*, 103–111; d) Y. Chen, W. Schuhmann, A. W. Hassel, *Electrochem. Commun.* **2009**, *11*, 2036–2039; e) Y. Chen, S. Milenkovic, A. W. Hassel, *ChemPhysChem* **2010**, *11*, 2838–2843; f) Y. Chen, A. W. Hassel, A. Erbe, *Electrocatalysis* **2011**, *2*, 106–113.

[3] a) J. Turkevich, P. C. Stevenson, J. Hillier, *Discuss. Faraday Soc.* **1951**, *11*, 55–75; b) G. Frens, *Nature Phys. Sci.* **1973**, *241*, 20–22.

[4] a) L. Chen, W. Cao, P. J. Quinlan, R. M. Berry, K. C. Tam, *ACS Sustainable Chem. Eng.* **2015**, *3*, 978–985; b) Y. Lv, Z. Lin, T. Tan, F. Svec, *Biotechnol. Bioeng.* **2014**, *111*, 50–58; c) Q. Cao, Y. Xu, F. Liu, F. Svec, J. M. J. Fréchet, *Anal. Chem.* **2010**, *82*, 7416–7421; d) S. Jain, D. G. Hirst, J. M. O'Sullivan, *Br. J. Radiol.* **2012**, *85*, 101–113.

[5] a) M. Stratakis, H. Garcia, *Chem. Rev.* **2012**, *112*, 4469–4506; b) P. Zhao, X. Feng, D. Huang, G. Yang, D. Astruc, *Coord. Chem. Rev.* **2015**, *287*, 114–136; c) H. Wang, Z. Dong, C. Na, *ACS Sustainable Chem. Eng.* **2013**, *1*, 746–752; d) J. He, W. Ji, L. Yao, Y. Wang, B. Khezri, R. D. Webster, H. Chen, *Adv. Mater.* **2014**, *26*, 4151–4155; e) J. Hu, Y. Dong, X. Chen, H. Zhang, J. Zheng, Q. Wang, X. Chen, *Chem. Eng. J.* **2014**, *236*, 1–8; f) L. Abahmane, A. Knauer, J. M. Köhler, G. A. Groß, *Chem. Eng. J.* **2011**, *167*, 519–526; g) H. Koga, T. Kitaoka, *Chem. Eng. J.* **2011**, *168*, 420–425.

[6] a) S. Liang, J. Jasinski, G. B. Hammond, B. Xu, *Org. Lett.* **2015**, *17*, 162–165; b) F. Zhu, H. Li, *Chin. J. Chem.* **2014**, *32*, 1072–1076.

[7] a) S. Panigrahi, S. Basu, S. Praharaj, S. Pande, S. Jana, A. Pal, S. K. Ghosh, T. Pal, *J. Phys. Chem. C* **2007**, *111*, 4596–4605; b) W. C. Ketchie, Y. Fang, M. S. Wong, M. Murayama, R. J. Davis, *J. Catal.* **2007**, *250*, 94–101.

[8] a) I. Nischang, O. Brüggemann, I. Teasdale, *Angew. Chem. Int. Ed.* **2011**, *50*, 4592–4596; *Angew. Chem.* **2011**, *123*, 4688; b) F. Alves, P. Scholder, I. Nischang, *ACS Appl. Mater. Interfaces* **2013**, *5*, 2517–2526; c) P. Scholder, I. Nischang, *Catal. Sci. Technol.* **2015**, *5*, 3917–3921.

[9] a) V. G. Minkina, S. I. Shabunya, V. I. Kalinin, V. V. Martynenko, A. L. Smirnova, *Int. J. Hydrogen Energy* **2012**, *37*, 3313–3318; b) R. Retnamma, A. Q. Novais, C. M. Rangel, L. Yu, M. A. Matthews, *Int. J. Hydrogen Energy* **2014**, *39*, 6567–6576.

[10] I. Nischang, T. J. Causon, *TrAC Trends Anal. Chem.* **2016**, *75*, 108–117.

Received: November 25, 2015
Published Online: February 4, 2016